Supporting Information: Combination of Solid State and Electrochemical Impedance Spectroscopy to Explore Effects of Porosity in Sol-Gel Derived $BaTiO_3$ Thin Films

Joshua Whittam,[1] Andrew L. Hector,[1*] Christopher Kavanagh,[2] John R. Owen[1] and Gillian Reid[1]

1 - University of Southampton, Chemistry, Highfield, SO17 1BJ, Southampton, UK.

2 - Deregallera Ltd, Unit 2 De Clare Court, Pontygwindy Industrial Estate, Caerphilly CF83 3HU, UK

Table S1: Literature survey of sol-gel derived $BaTiO_3$ films in which solid state impedance has been used to measure the dielectric constant of the film.

Deposition method	Film thickness/ µm	Dielectric constant	Number of coatings	Annealing temperature / °C
Spin Coated[1]	0.11	85	4	600
Dip Coating[2]	0.25	230	7	650
Spin Coated[3]	0.38	370	3	700
Dip Coating[4]	0.40	390	3	850
Spin Coated[5]	0.40	370	3	700
Dip Coating[6]	0.50	800	7	650
Spin Coated[7]	0.50	318	5	800
Dip Coating[2]	0.58	1000	20	650
Spin Coated[8]	2.50	521	12	750
Dip Coating[4]	3.00	630	10	850

Table S2 Integration of the EDS map shown in Figure 2c performed on the region of a pinhole in a $BaTiO_3$ film.

Element	Oxygen	Silicon	Titanium	Barium	Platinum	**Total%**
Weight%	12.6	5.1	15.5	43.6	22.8	99.6
Atom%	45.0	10.3	18.5	18.1	6.7	98.5

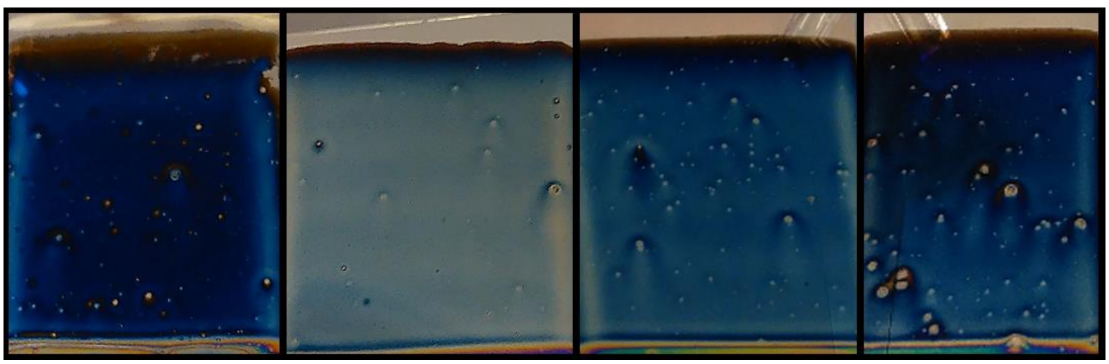

Figure S1 Images of $BaTiO_3$ thin films deposited with a single dip from 1 day aged sols containing (left to right) 2, 4, 8 and 15 mL deionised H_2O and annealed at 750 °C.

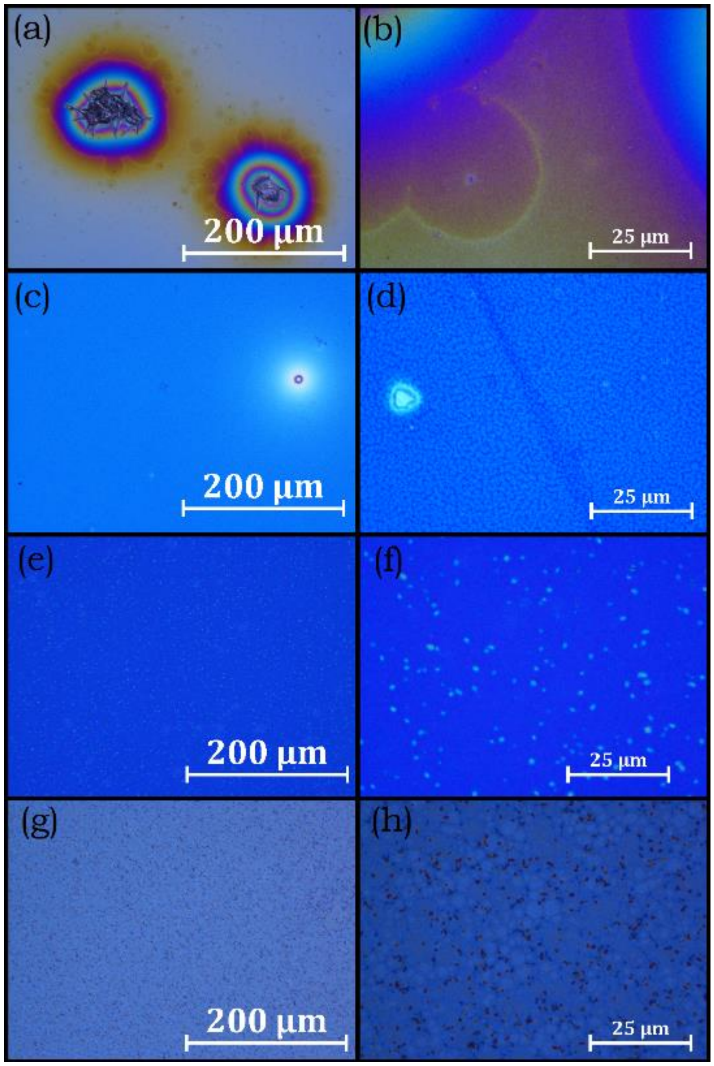

Figure S2 Optical microscopy of $BaTiO_3$ thin films deposited with a single dip and annealed at 750 °C at 20× (left) and 100× (right) magnification): (a) and (b) 1 mL of H_2O, 1 day aged at 250 rpm; (c) and (d) 4 mL of H_2O, 1 day aged at 250 rpm; (e) and (f) 4 mL of H_2O, 6 days aged at 250 rpm; (g) and (h) 4 mL of H_2O, 6 days aged at 1000 rpm.

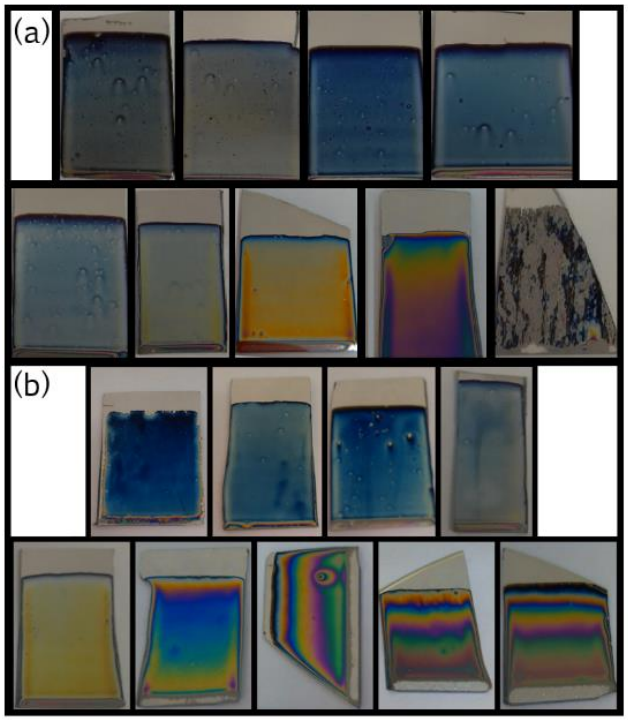

Figure S3 (a) Thin films of $BaTiO_3$ produced from sols containing 4 mL of H_2O aged for 1, 2, 3, 4, 5, 6, 7, 8 or 9 days (top left to bottom right) and annealed at 750 °C. The equivalent sequence with stirring at 1000 rpm is shown in (b).

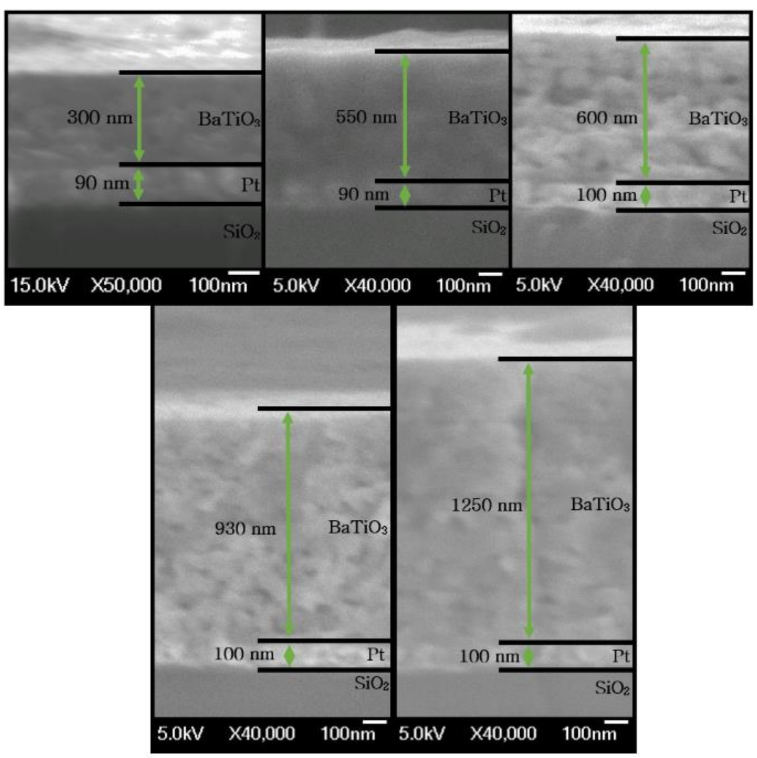

Figure S4 Cross sectional SEM of $BaTiO_3$ films produced with 1 (top left), 2 (top centre), 3 (top right), 4 (bottom left) or 5 (bottom right) iterations of dip and anneal 750 °C.

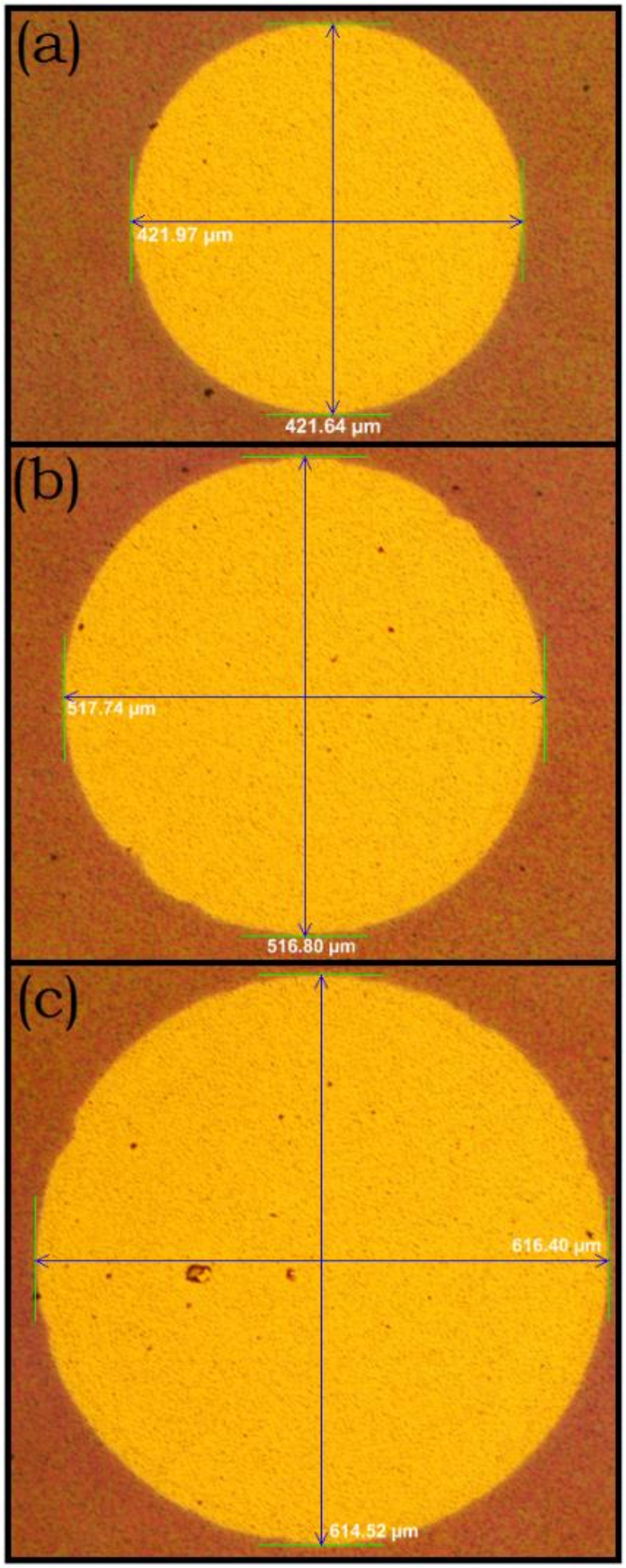

Figure S5 Image of Au contacts evaporated onto a 3 dip and anneal cycle $BaTiO_3$ film with diameters of (a) 0.4 mm, (b) 0.5 mm, and (c) 0.6 mm.

Table S3 The capacitances and calculated effective permittivity of a 3 dip and anneal cycle $BaTiO_3$ film extracted by fitting the Nyquist and Bode plots of the impedance data using ZView.

Pad Size	**Diameter / mm**	**Area / mm^2**	**Capacitance / nF**	**Areal Capacitance / µF cm^{-2}**	**Effective Permittivity**
0.4 mm (1)	0.420	0.139	0.584(11)	0.421	286
0.4 mm (2)	0.420	0.139	0.55(3)	0.398	270
0.4 mm (3)	0.420	0.139	0.582(12)	0.420	285
0.5 mm (1)	0.515	0.208	0.908(17)	0.436	295
0.5 mm (2)	0.515	0.208	0.914(19)	0.439	297
0.5 mm (3)	0.515	0.208	0.914(19)	0.439	297
0.6 mm (1)	0.615	0.297	1.31(17)	0.442	296
0.6 mm (2)	0.615	0.297	1.30(19)	0.436	296
0.6 mm (3)	0.615	0.297	1.25(16)	0.420	285

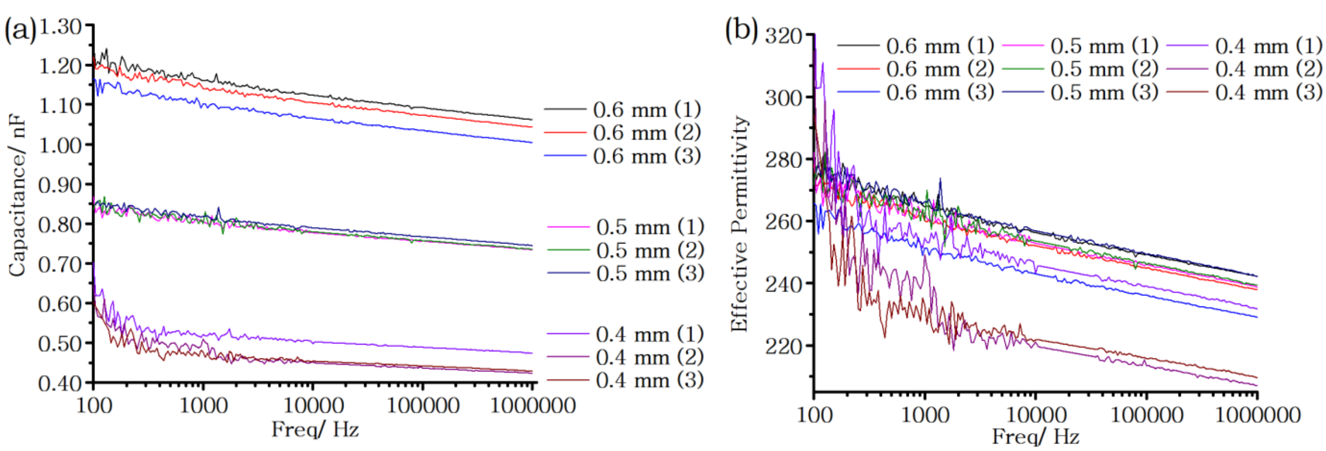

Figure S6 The change in capacitance (a) and the effective permittivity (b) as a function of frequency.

Table S4 The capacitances and calculated effective permittivity of a 3 dip and anneal cycle $BaTiO_3$ film extracted averaging the capacitance across and applied frequency range (SI, Figure S16).

Pad Size	**Diameter / mm**	**Area / mm^2**	**Capacitance / nF**	**Areal Capacitance / µF cm^{-2}**	**Effective Permittivity**
0.4 mm (1)	0.420	0.139	0.508	0.367	249
0.4 mm (2)	0.420	0.139	0.461	0.333	225
0.4 mm (3)	0.420	0.139	0.457	0.330	223
0.5 mm (1)	0.515	0.208	0.781	0.375	254
0.5 mm (2)	0.515	0.208	0.783	0.376	255
0.5 mm (3)	0.515	0.208	0.781	0.380	258
0.6 mm (1)	0.615	0.297	1.13	0.380	257
0.6 mm (2)	0.615	0.297	1.11	0.374	253
0.6 mm (3)	0.615	0.297	1.07	0.360	244

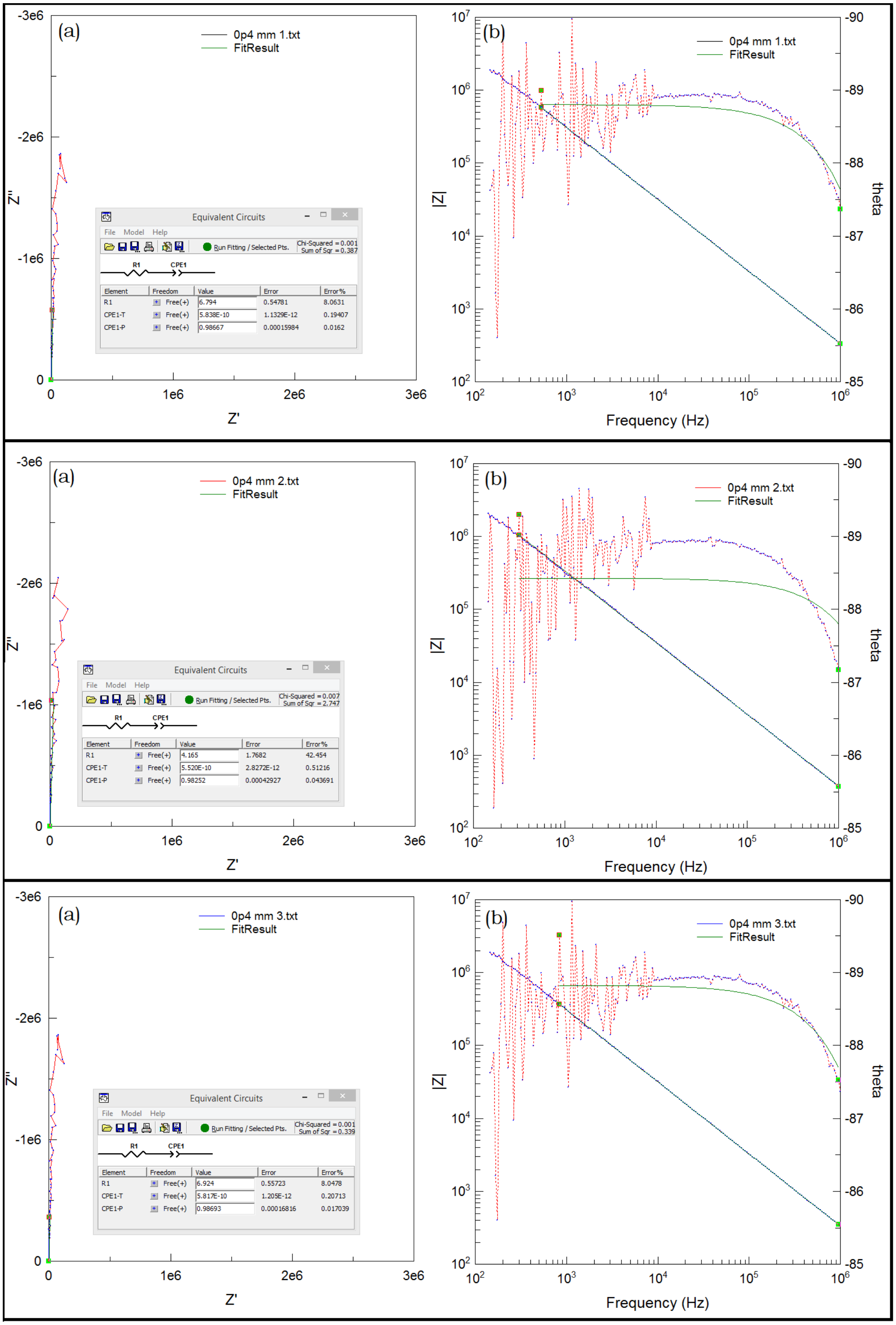

Figure S7 Fittings to the Nyquist (a) and Bode (b) plots of the solid state impedance data for a $BaTiO_3$ thin film produced by dipping and annealing at 750 °C 3 times: using a 0.4 mm pad diameter.

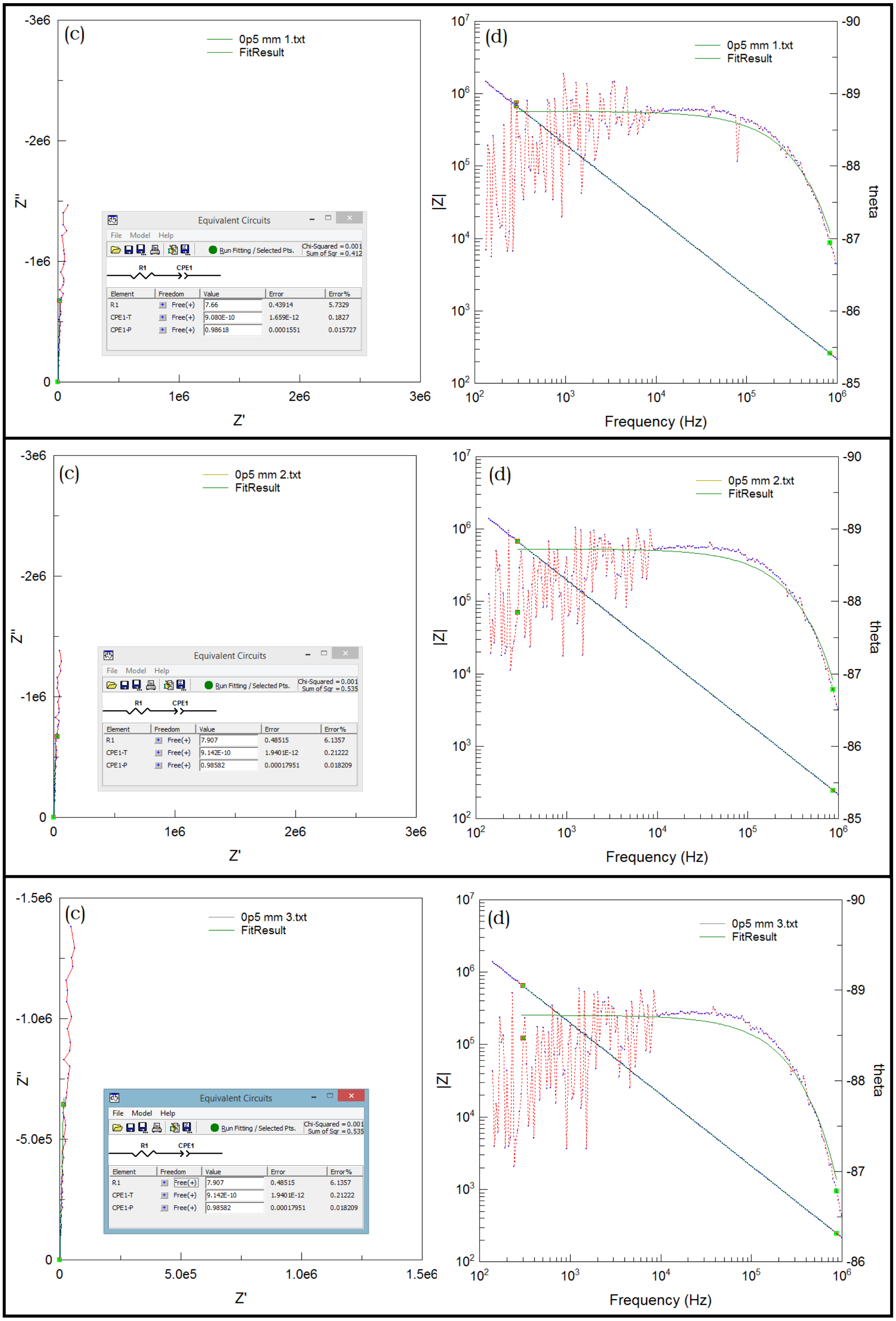

Figure S8 Fittings to the Nyquist (c) and Bode (d) plots of the solid state impedance data for a $BaTiO_3$ thin film produced by dipping and annealing at 750 °C 3 times: using a 0.5 mm pad diameter.

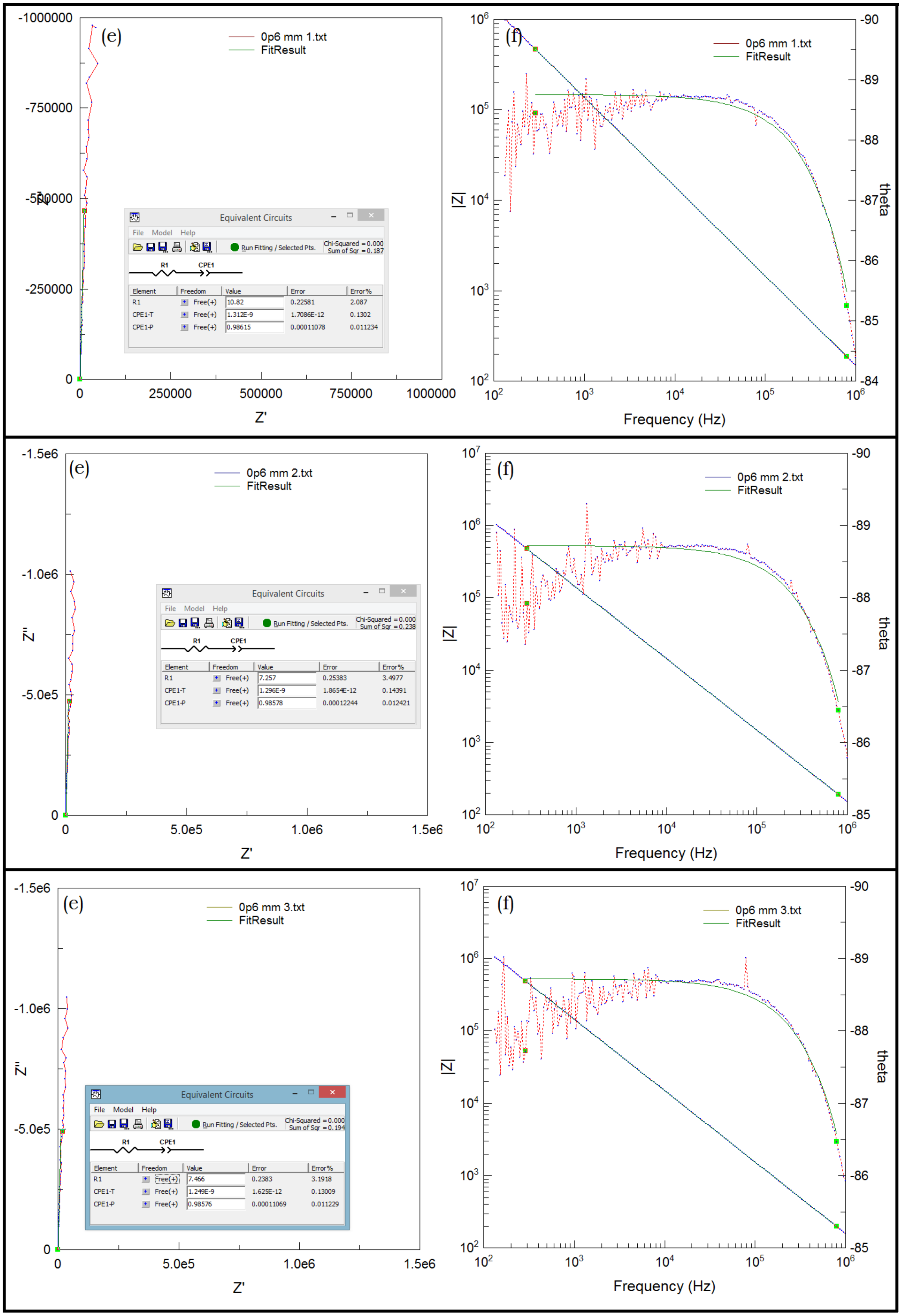

Figure S9 Fittings of the Nyquist (e) and Bode (f) plots of the solid state impedance data for a $BaTiO_3$ thin film produced by dipping and annealing at 750 °C 3 times: using a 0.4 mm pad diameter.

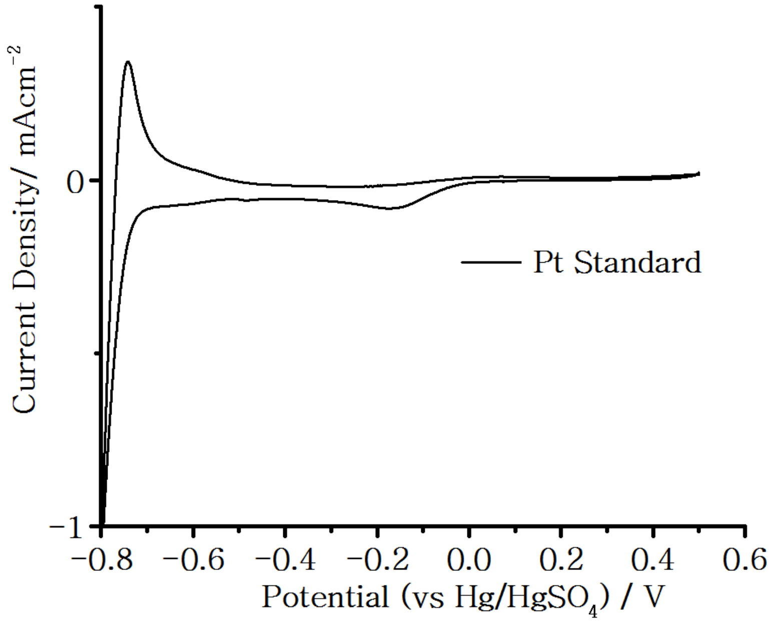

Figure S10 Cyclic voltammograms of the Si/Pt substrate, with a scan rate of 100 mV s^{-1}, a Pt gauze counter electrode and a Hg/$HgSO_4$ reference electrode were used with a non- aerated 0.5 mol dm^{-3} K_2SO_4 electrolyte.

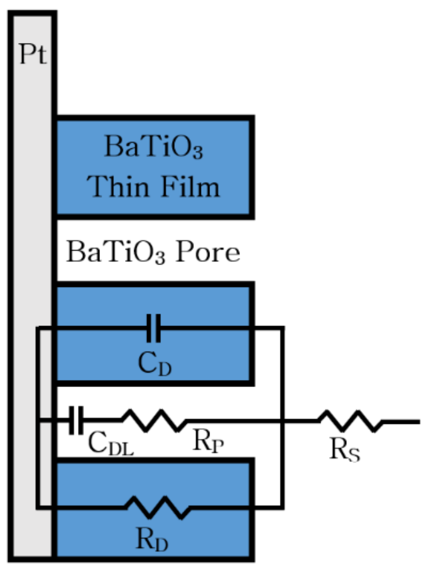

Figure S11 Equivalent circuit describing a porous dielectric film on a platinum electrode, where R_S is uncompensated solution resistance, C_{DL} is double layer capacitance, C_D is dielectric capacitance, R_P is pore resistance and R_D is dielectric resistance.

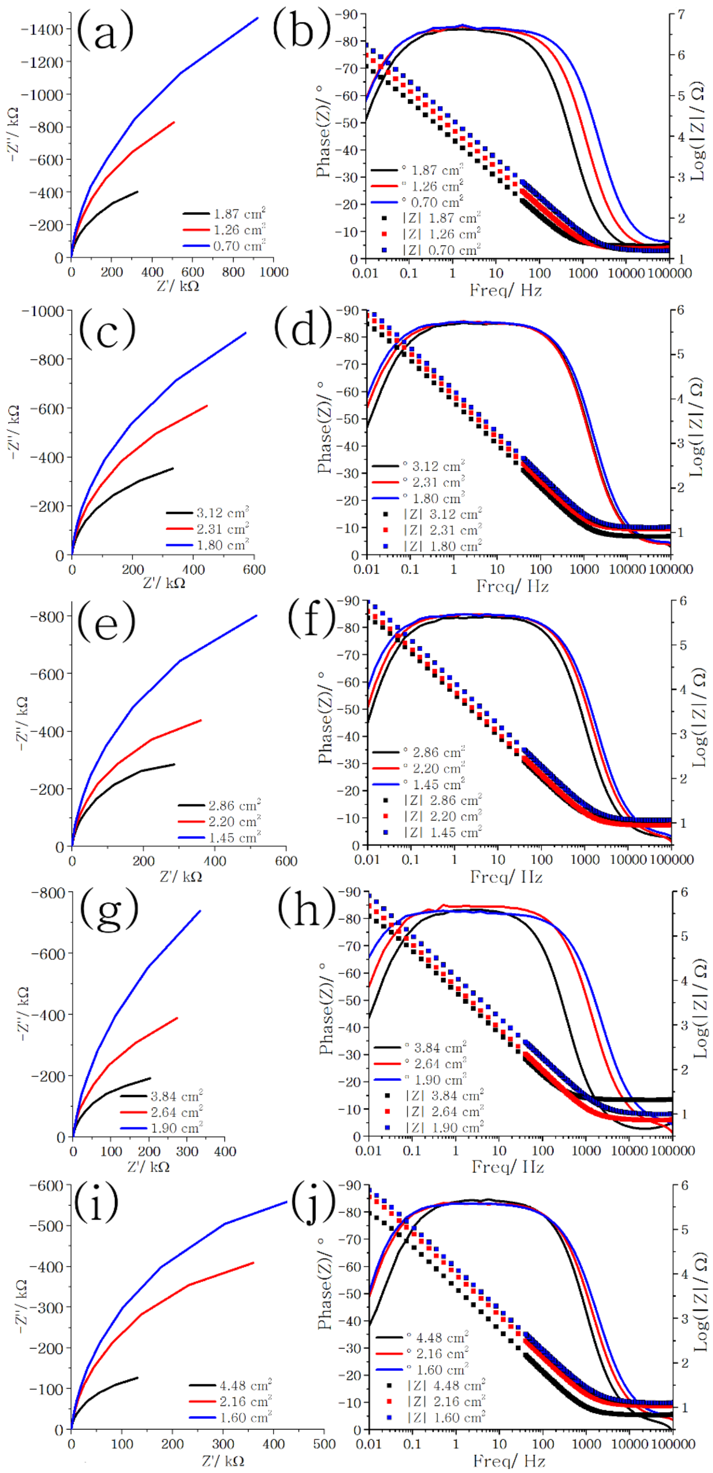

Figure S12 Nyquist plots (left) and Bode plots (right) of the electrochemical impedance data for $BaTiO_3$ films on Pt film substrates produced by dipping and annealing at 750 °C: (a) and (b) 1 cycle; (c) and (d) 2 cycles; (e) and (f) 3 cycles; (g) and (h) 4 cycles; (i) and (j) 5 cycles. Data were collected in 0.5 mol dm^{-3} K_2SO_4 (20 mL) with a Pt gauze counter electrode and a $Hg/HgSO_4$ (sat. K_2SO_4) reference electrode. A sinusoidal potential with 10 mV amplitude was applied at frequencies from 0.1 MHz to 10 mHz. The area exposed to the electrolyte is indicated, fittings are shown in Figs. S11-S15.

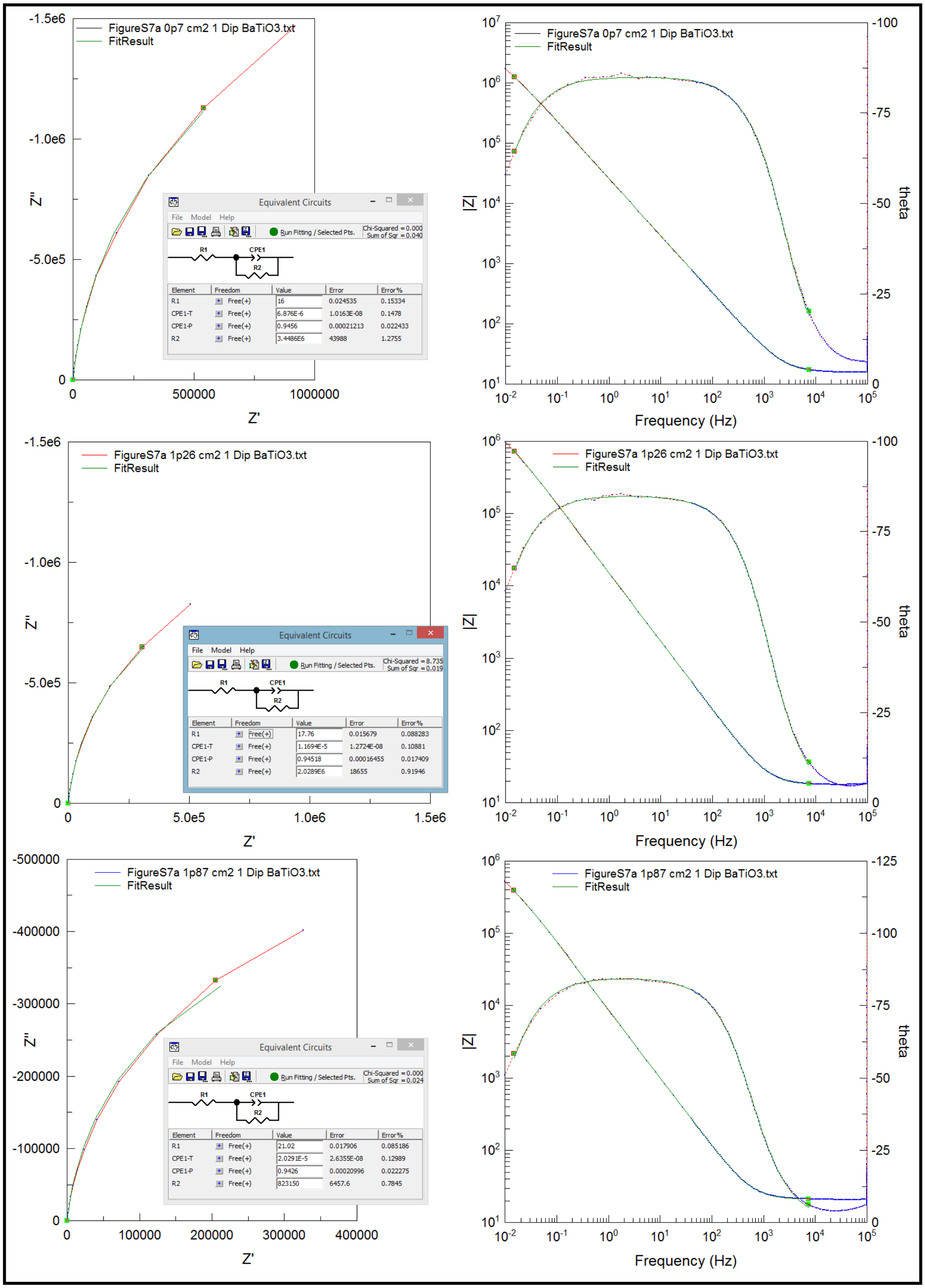

Figure S13 Fits to the Nyquist (left) and Bode (right) plots of the electrochemical impedance for $BaTiO_3$ films on Pt film substrates produced by 1 cycle of dipping and annealing at 750 °C (SI, Figure S10a–S10b).

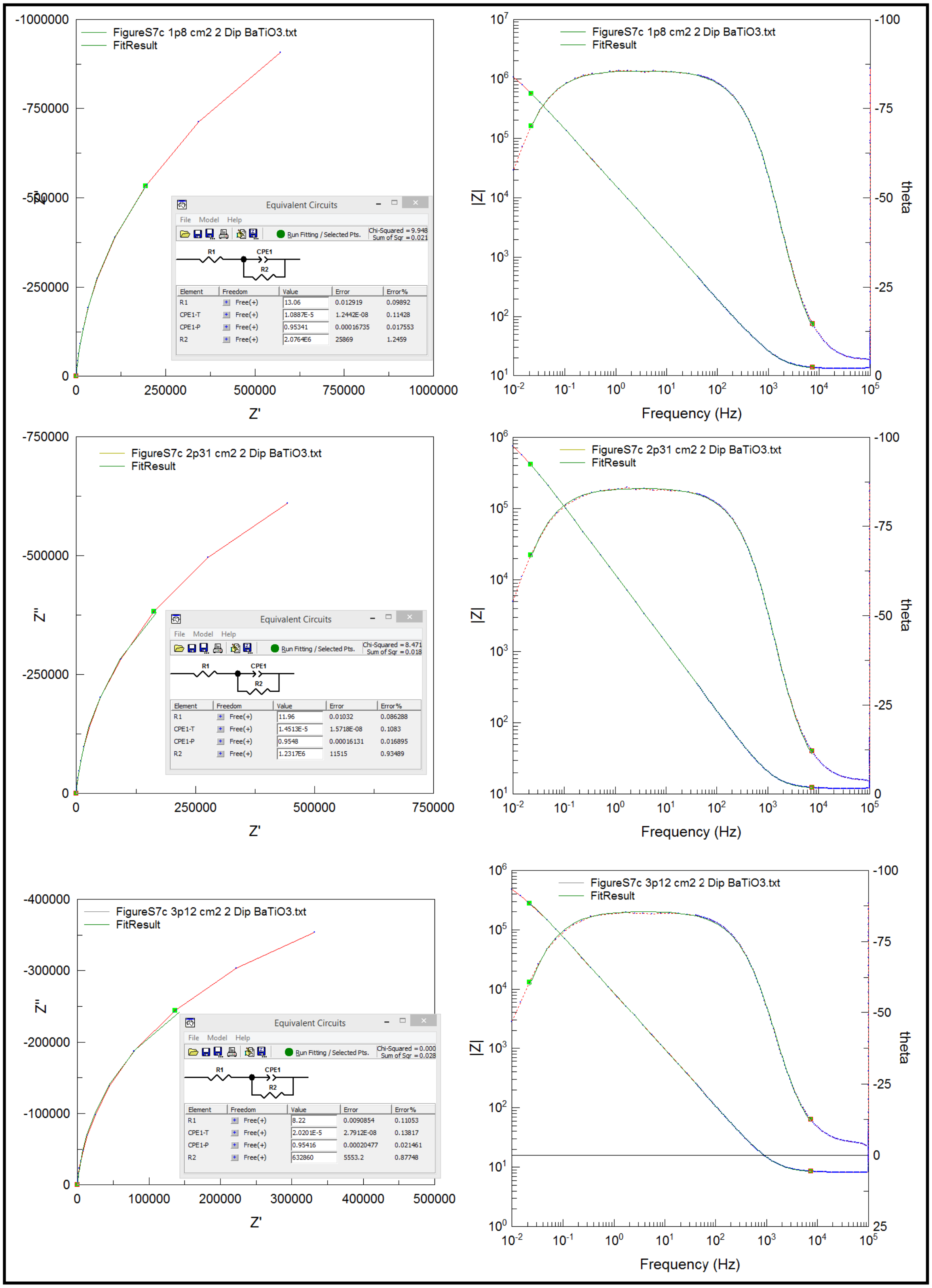

Figure S14 Fits to the Nyquist (left) and Bode (right) plots of the electrochemical impedance for $BaTiO_3$ films on Pt film substrates produced by 2 cycles of dipping and annealing at 750 °C (SI, Figure S10c-S10d).

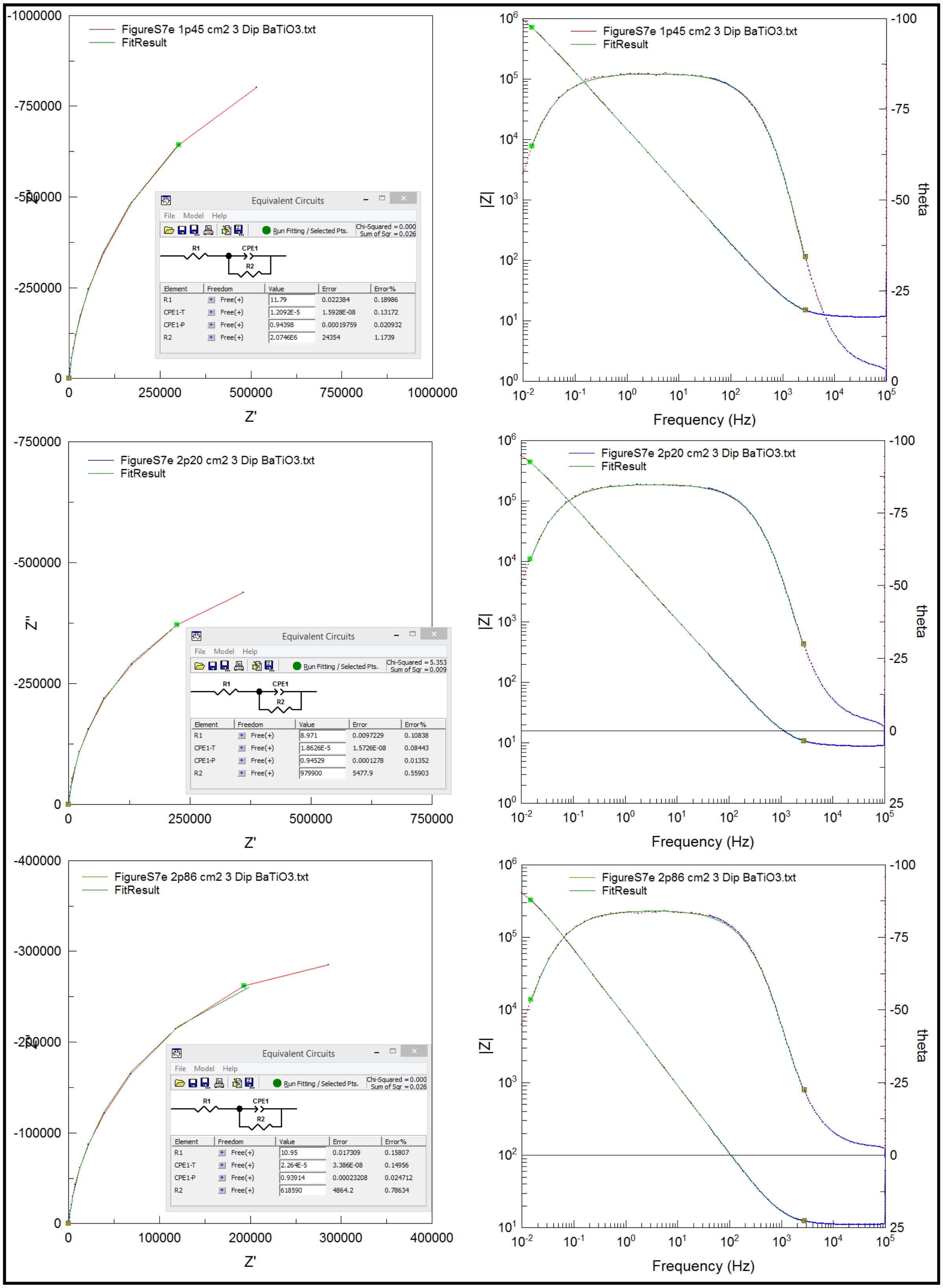

Figure S15 Fits to the Nyquist (left) and Bode (right) plots of the electrochemical impedance for $BaTiO_3$ films on Pt film substrates produced by 3 cycles of dipping and annealing at 750 °C (Figure S10e–S10f).

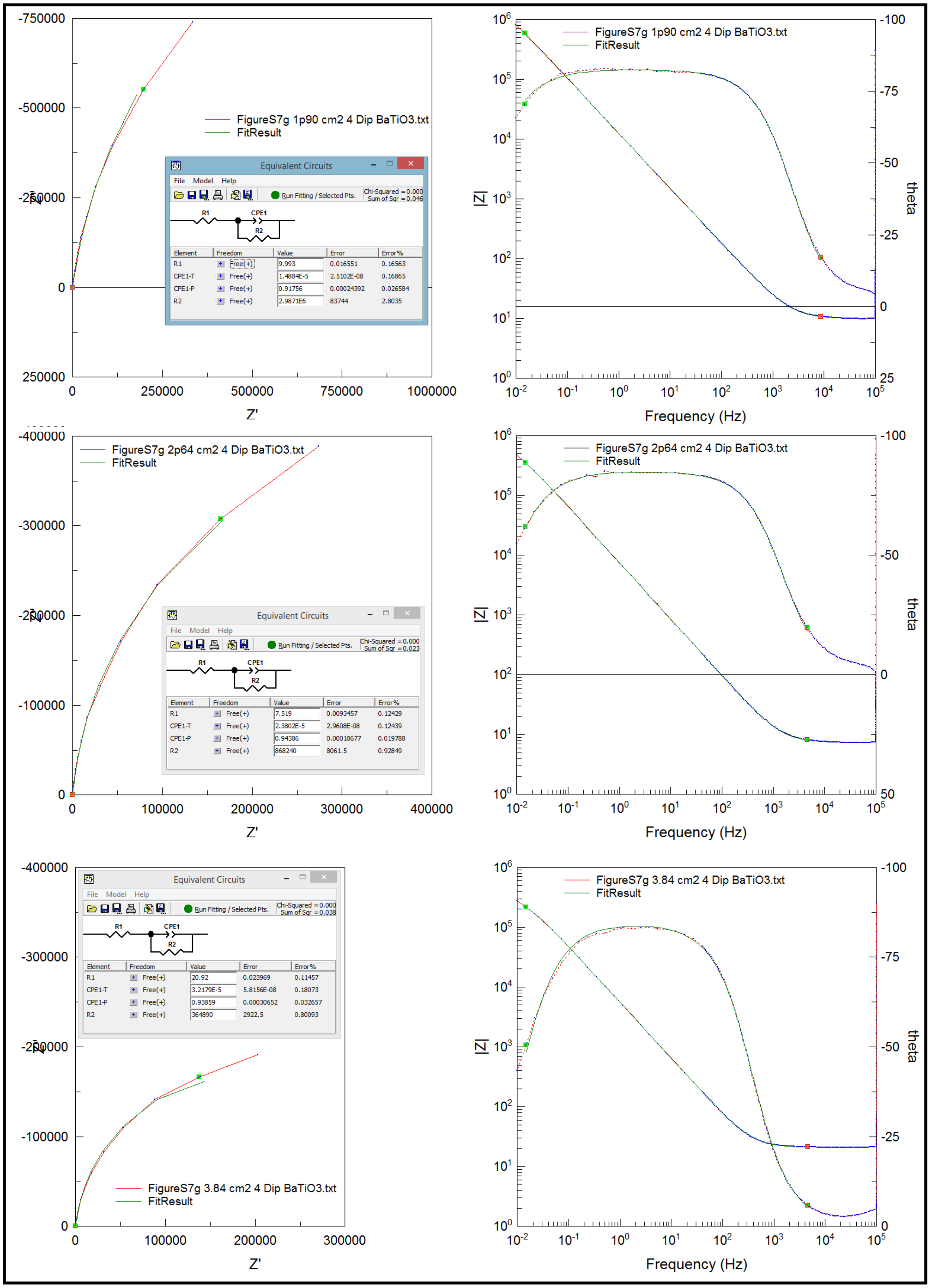

Figure S16 Fits to the Nyquist (left) and Bode (right) plots of the electrochemical impedance for $BaTiO_3$ films on Pt film substrates produced by 4 cycles of dipping and annealing at 750 °C (Figure S10g–S10h).

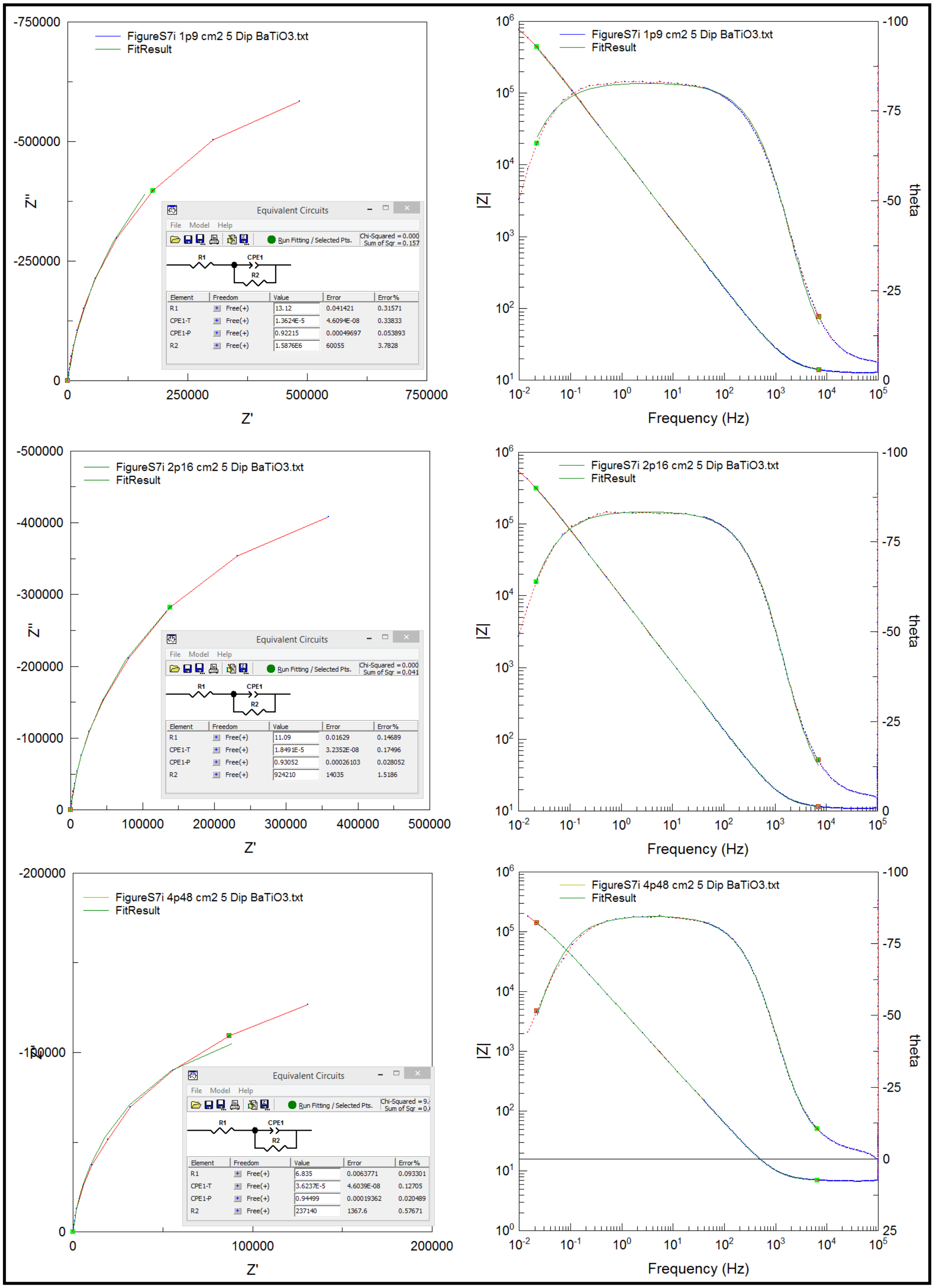

Figure S17 Fits to the Nyquist (left) and Bode (right) plots of the electrochemical impedance for $BaTiO_3$ films on Pt film substrates produced by 5 cycles of dipping and annealing at 750 °C (Figure S10i–S10j).

Table S5 Fitted parameters from the electrochemical impedance of $BaTiO_3$ films on Pt film substrates produced by dipping and annealing at 750 °C 1, 2, 3, 4 or 5 times. Data were collected in 0.5 mol dm^{-3} K_2SO_4 (20 mL) with a Pt gauze counter electrode and a Hg/$HgSO_4$ (sat. K_2SO_4) reference electrode. A sinusoidal potential with 10 mV amplitude was applied at frequencies from 0.1 MHz to 10 mHz. The area exposed to the electrolyte is indicated. Fits are shown in Figs. S11-S15.

Number of coating Iterations	Area exposed / cm^2	Dielectric resistance / MΩ	Solution resistance / Ω	Capacitance / µF	Areal Capacitance / µF cm^{-2}
1	1.87	0.823(6)	21.020(16)	20.3(3)	10.8
1	1.26	2.028(18)	17.760(16)	11.69(12)	9.28
1	0.70	3.45(4)	16.010(24)	6.88(10)	9.82
2	3.12	0.633(6)	8.220(9)	20.20(3)	6.47
2	2.31	1.232(11)	11.960(10)	14.513(16)	6.28
2	1.80	2.08(3)	13.060(13)	10.887(12)	6.05
3	2.86	0.619(5)	10.950(2)	22.64(3)	7.92
3	2.20	0.980(5)	8.97(10)	18.626(16)	8.47
3	1.45	2.07(2)	11.79(2)	12.092(16)	8.37
4	3.84	0.365(3)	20.92(2)	32.18(6)	8.38
4	2.64	0.868(8)	7.52(9)	23.80(3)	9.02
4	1.90	2.99(8)	9.99(16)	14.88(3)	7.83
5	4.48	0.2371(14)	6.835(6)	36.24(4)	8.09
5	2.16	0.92(14)	11.090(16)	18.49(3)	8.56
5	1.60	1.59(6)	13.12(4)	13.62(5)	8.52

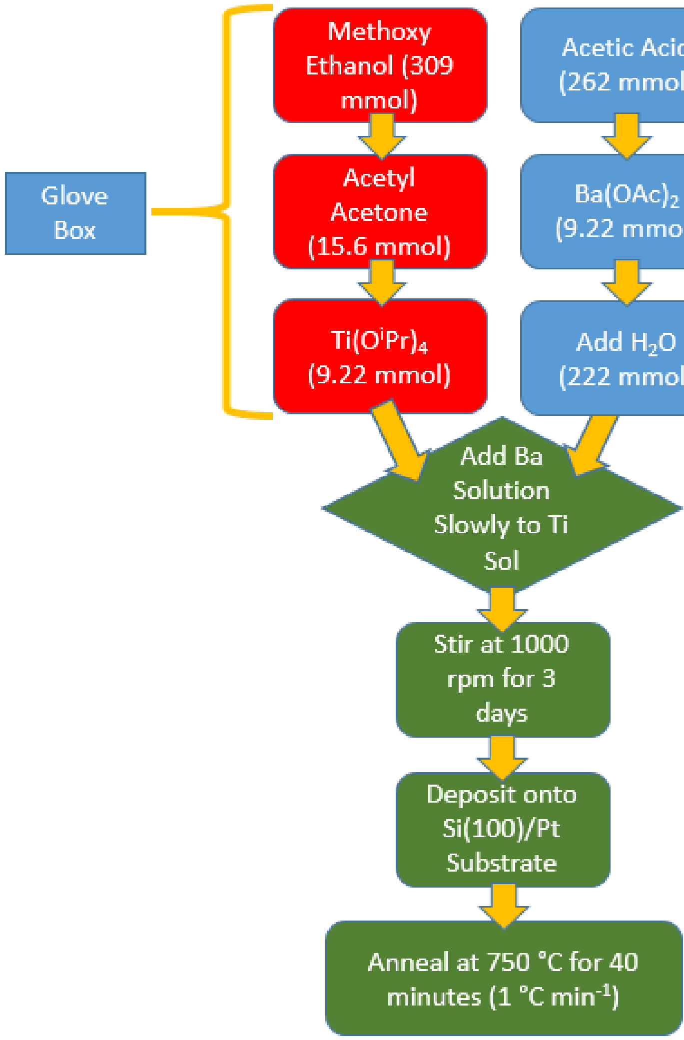

Figure S18 Flowchart describing the production of a $BaTiO_3$ precursor sol.

References

(1) Huang, L.; Chen, Z.; Wilson, J. D.; Banerjee, S.; Robinson, R. D.; Herman, I. P.; Laibowitz, R.; O'Brien, S. Barium Titanate Nanocrystals and Nanocrystal Thin Films: Synthesis, Ferroelectricity, and Dielectric Properties. *J. Appl. Phys.* **2006**, *100* (3), 034316 (10 pages).

(2) Hayashi, T.; Oji, N.; Maiwa, H. Film Thickness Dependence of Dielectric Properties of BaTiO3 Thin Films Prepared by Sol-Gel Method. *Jpn. J. Appl. Phys.* **1994**, *33* (Part 1, No. 9B), 5277–5280.

(3) Sharma, H. B.; Mansingh, A. Phase Transition in Sol-Gel-Derived Barium Titanate Thin Films. *J. Phys. D. Appl. Phys.* **1998**, *31* (13), 1527–1533.

(4) Kumazawa, H.; Masuda, K. Fabrication of Barium Titanate Thin Films with a High Dielectric Constant by a Sol-Gel Technique. *Thin Solid Films* **1999**, *353*, 144–148.

(5) Sharma, H. B.; Sarma, H. N. K.; Mansingh, A. Ferroelectric and Dielectric Properties of Sol-Gel Processed Barium Titanate Ceramics and Thin Films. *J. Mater. Sci.* **1999**, *34*, 1385–1390.

(6) Hayashi, T.; Ohji, N.; Hirohara, K.; Fukunaga, T.; Maiwa, H. Preparation and Properties of Ferroelectric BaTiO3 Thin Films by Sol-Gel Process. *Jpn. J. Appl. Phys.* **1993**, *32* (Part 1, No. 9B), 4092–4094.

(7) Lee, B.; Zhang, J. Preparation, Structure Evolution and Dielectric Properties of BaTiO3 Thin Films and Powders by an Aqueous Sol–gel Process. *Thin Solid Films* **2001**, *388* (1–2), 107–113.

(8) Kamalasanan, M. N.; Kumar, N. D.; Chandra, S. Dielectric and Ferroelectric Properties of BaTiO3 Thin Films Grown by the Sol-Gel Process. *J. Appl. Phys.* **1993**, *74* (9), 5679–5686.